

Effect of Post Heat Treatment on Fatigue Strength of AlSi10Mg Produced by Laser Powder Bed Fusion Process



Wei-Jen Lai, Avinesh Ojha, and Ziang Li

Abstract The effect of the post heat treatment on the fatigue properties was investigated for AlSi10Mg aluminum alloy produced by laser powder bed fusion process. The post heat treatments focused on in this study are stress relief (300 °C for 2 h), solutionization (540 °C for 2 h), T6 (540 °C for 2 h and 180 °C for 8 h), and T5 (120 °C, 150 °C, and 200 °C). Quasi-static tensile tests and hardness tests were performed on samples with different post heat treatments and the mechanical properties were compared. Fatigue tests were then performed on the same samples to understand the relation between static mechanical properties (yield strength, ultimate tensile strength (UTS), and hardness) and the fatigue strength. The results show that the as-built samples (no post heat treatment) have the highest UTS (398 MPa) while the T6 samples have the highest yield strength (240 MPa). The solutionized samples have the lowest UTS and yield strength (205 MPa and 95 MPa, respectively), as expected. The hardness has a positive correlation with the UTS, not the yield strength. The fatigue test results show that the as-built samples have the highest fatigue strength (154 MPa) and the T6 heat treatment did not improve the fatigue strength. Besides, the stress relieved samples have a fatigue strength (88 MPa) close to the T6 samples (78 MPa). T5 aging curves show mild age hardening behavior. No significant change in silicon eutectic morphology was observed at all T5 aging temperatures investigated. Strong location dependency of hardness was observed in as-built samples due to thermal exposure during the building process. In summary, the static tensile mechanical properties do not show a correlation to the fatigue strength for AlSi10Mg under different post heat treatments. The post heat treatment should be tailored to meet the requirement based on the application needs.

Keywords Fatigue · Post heat treatment · AlSi10Mg · Laser powder bed fusion

W.-J. Lai (✉) · A. Ojha · Z. Li
Ford Motor Company, Dearborn, MI, USA

Introduction

Metal additive manufacturing (AM) has gained considerable interest in recent years as it offers the possibilities of fabricating near net shape parts with complex geometries which are difficult to build using traditional manufacturing processes. Laser powder bed fusion (L-PBF) process has the advantage over other metal AM processes because of its high dimensional accuracy and low defect volume. Parts produced by L-PBF process have superior yield strength (YS) and ultimate tensile strength (UTS) in the as-built condition. Among the few materials available for L-PBF process, AlSi10Mg is widely used and studied owing to the good process stability and near-full-dense microstructure. However, due to the high silicon content, the microstructure is very sensitive to temperature, so are the mechanical properties. In many circumstances, post heat treatment is deemed necessary to remove the substantial residual stress in the as-built parts. Without properly stress relieving the as-built part before removing from the build plate, severe distortion and cracking can occur. The residual stress can also deteriorate the fatigue performance of the parts. Hence parts under as-built condition are rarely used in real applications.

As mentioned earlier, post heat treatment can significantly alter the microstructure and the mechanical performance. Most literatures reported that the as-built L-PBF AlSi10Mg parts have the highest UTS and hardness [1–5], which means post heat treatments only decrease the UTS through coarsening the silicon eutectic. However, some researchers reported that the artificial aging, ex. T5 or T6, can improve UTS, YS, or hardness. Note that these three mechanical properties (UTS, YS, and hardness) do not always follow the same trend. For instance, a material can have a lower UTS but a higher YS than another material. Hence, it is important to compare all three mechanical properties for materials with heat treatments. Zhou et al. [6] reported a hardness increase from 94.4 HV to 103.4 HV as well as a yield strength increase from 194.7 MPa to 268.5 MPa, for the as-built and T6 (520 °C/2 h and 160 °C/10 h) samples, respectively, for L-PBF AlSi10Mg. Fousová et al. [7] reported that T5 temperature between 120 °C and 180 °C can significantly increase the hardness from approximately 125 HV to 140 HV for L-PBF AlSi10Mg. The 160 °C T5 samples (160 °C/5 h) have a yield strength of 268 MPa compared to 255 MPa of the as-built samples. However, the UTS is lower (342 MPa) than the as-built samples (377 MPa). The T6 heat treatment (510 °C/6 h and 170 °C/4 h) however decreases both the UTS (284 MPa) and yield strength (210 MPa) compared to the as-built samples. Kempen et al. [8] reported an increase of hardness from 136 HV to 152 HV after T5 (175 °C/6 h) heat treatment for L-PBF AlSi10Mg but no change in UTS was observed. Tradowsky et al. [9] reported an increase in yield strength and a decrease in UTS after T6 heat treatment (530 °C/5 h and 160 °C/12 h) for vertically built L-PBF AlSi10Mg with as-fabricated surface. Brandl et al. [10] reported increase in UTS for both vertically and horizontally built L-PBF AlSi10Mg samples after T6 (525 °C/6 h and 165 °C/7 h) heat treatment.

The discrepancy in mechanical properties seen by different researchers might be attributed to the thermal history in the local material, which is largely affected by the

process parameters. The thermal history experienced by the local material during the building process can be seen as “in-situ” heat treatment. In other words, the samples have gone through a series of heat treatments in the so-called as-built condition. It makes comparing mechanical properties and effect of heat treatment across samples from different literatures extremely difficult since they do not have an equal starting point.

It is well accepted that the higher the hardness, the higher the UTS and fatigue strength for the same material provided that the surface condition and defect characteristics are the same [11]. Thus, the hardness increase has a strong implication on the fatigue strength increase. Since fatigue testing requires a long time and special equipment, most literatures provide only UTS or hardness data for post heat treatment analysis. Limited fatigue data are available for L-PBF AlSi10Mg to understand the effect of post heat treatment. Besides, a debate on whether the post heat treatment is beneficial to fatigue properties exist among the available fatigue data [4, 10, 12–14]. Therefore, the effect of post heat treatment on fatigue properties needs to be further analyzed such that proper post heat treatment can be determined based on the design needs.

In this paper, the effects of common post heat treatments were investigated. Quasi-static tensile properties were studied for samples under stress relieved, solutionized, and T6 conditions. Aging curves were obtained for T5 and T6 conditions. Fatigue tests were performed for samples under stress relieved and T6 conditions. Results were compared with the as-built conditions to understand the effects of post heat treatments. Microstructure evolution of the silicon morphology was also studied in order to correlate with the mechanical properties.

Experimental Procedure

Sample Preparation

AlSi10Mg aluminum alloy is selected for this study. The alloy composition is listed in Table 1. Samples were built using SLM 500 by SLM Solutions with the tensile axis in the Z direction (vertical direction) with optimum process parameters (Table 2) to minimize the porosity. An inside-out scan strategy was adopted, which hatches the center portion, then a contour scan and border scan on the outer part to reduce the potential for porosity formation at the edge. The rotation between each layer for hatching is 67°. The samples were built into cylindrical rod shape with 13 mm and 15 mm diameters for tensile and fatigue samples, respectively. Tensile and fatigue samples were then machined from the rods into the standard test coupons, as shown in Fig. 1a, b, respectively. The tensile and fatigue sample geometries are based on ASTM E8 [15] and ASTM E466 [16], respectively. Fatigue samples were mechanically polished along the axial direction to remove machining marks.

Table 1 Composition of AISi10Mg powder

	Si(%)	Fe(%)	Cu(%)	Mg(%)	Cr(%)	Ni(%)	Ti(%)	Ca(%)	Ga(%)	Sr(ppm)	V(%)	Al(%)
AISI10Mg	10.48	0.125	0.0057	0.291	0.012	0.0108	0.129	0.0059	0.0123	142	0.0146	88.8

Table 2 Summary of laser parameters

Region	Power (W)	Speed (mm/s)	Hatch spacing (mm)	Layer thickness (mm)	Built plate temperature (°C)
Border & Contour	300	730	0.17	0.03	200
Hatch	370	1975			

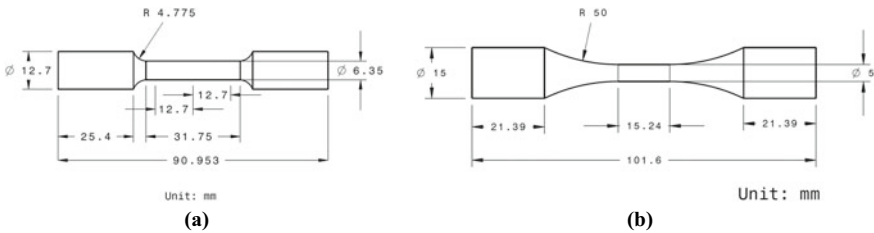


Fig. 1 a Tensile and b fatigue sample geometries

Heat Treatment

A series of post heat treatments were performed and summarized in Table 3. The types of tests performed are also listed for reference. As-built samples are without any post heat treatment and are denoted as AB. Solutionized samples (denoted as SHT) were heated at 540 °C for 2 h and then quenched in water to obtain homogenized microstructure and uniform mechanical properties. Stress relieved samples (denoted as SR) are heated at 300 °C for 2 h to remove most of the residual stress produced during the building process. T5 aging was performed at 120 °C, 150 °C, and 200 °C for various hours. One sample was used for each aging curve and samples were sectioned at various locations from the fatigue samples. For instance, the hardness was measured from a sample before heat treatment. The sample was then heated to the target temperature for the pre-determined hours and quenched in water. At

Table 3 Summary of the post heat treatments and the corresponding mechanical tests performed in this study

Sample ID	Description	Heat treatment	Tensile	Fatigue	Hardness
AB	As-built	NA	✓	✓	✓
SHT	Solution heat treatment	540 °C/2 h	✓		✓
SR	Stress relief	300 °C/2 h	✓	✓	✓
T5	Artificial aging	120 °C, 150 °C, 200 °C			✓
T6	Solution heat treatment + Artificial aging	540 °C/2 h + 180 °C/8 h	✓	✓	✓

least 5 hardness values were measured for each sample, and the process repeats until the whole aging curve is finished. Small pieces where hardness was measured were cut from the sample at different aging time for later microstructure observation. The benefit of using one single sample to generate the aging curve is that it can significantly reduce the hardness measurement scatter due to possible microstructure inhomogeneity and non-uniform mechanical properties commonly seen in L-PBF materials. For T6 aging curve, the sample was first sectioned into multiple pieces; One was used for initial hardness reference. The others were solutionized at 540 °C for 2 h and quenched in water. Individual homogenized pieces were artificially aged at 160 °C and 200 °C for various hours. The peak aged samples were aged at 180 °C for 8 h and denoted as T6. Note that the samples used in the T5 and T6 aging curves are made in SLM125 from previous study and have a higher hardness in the as-built state [17].

Thermal exposure was performed at 250 °C and 300 °C to understand the change in mechanical properties at elevated temperature. The samples were kept at the target temperature in air for various hours. Samples were quenched in water at each time interval and the hardness values were recorded. The same sample was used for each thermal exposure curve to minimize scatter. Note that the samples used in the thermal exposure study are made in SLM125 from previous study and have a higher hardness in the as-built state [17].

Tensile Test and High Cycle Fatigue (HCF) Test

The tensile tests were conducted using MTS servo-hydraulic test system with a 100 kN load cell at room temperature and normal lab atmosphere following ASTM E8 standard [15]. The displacement rate is 0.19 mm/min up to 1 mm and increases to 1 mm/min until the sample is fully separated.

Uniaxial fatigue tests were performed at stress ratio $R = -1$ and 60 to 70 Hz following ASTM E466 [16]. MTS servo-hydraulic fatigue testing machines with a 25 kN load cell were used for the tests. Tests were conducted in normal lab air at room temperature. Samples were tested until full separation or until 10^7 cycles (runout).

In this study, the fatigue S–N curves were fitted using random fatigue limit (RFL) model [18] with the aid of maximum likelihood method described in [19] to account for the runout data points. The equation is shown below.

$$S_a - S_L = C(2N_f)^b \quad (1)$$

where S_a is the stress amplitude, S_L is the infinite-life fatigue limit of the material, N_f is the number of cycles to fracture, and C and b are empirical constants. The fatigue strength is then calculated at 10^7 cycles. The model can properly capture the changing slope of the fatigue S–N curve in log–log scale.

Hardness Measurement and Microstructure Analysis

The microhardness measurement was conducted using LECO Microhardness Tester LM 248 with a load of 300 g and a dwell time of 13 s. Samples were sectioned and cold mounted in epoxy. Total 5 indentations were measured for each case.

Hardness profiles along the axial direction of a few post-test fatigue samples were obtained to understand the location dependency of mechanical properties for L-PBF AlSi10Mg. Hardness was measured at equal distance from the top to the bottom of the vertically built fatigue samples. Note that the measurement was performed on the XY plane of the fatigue sample. The fatigue sample was sectioned into multiple pieces on which the hardness measurement was performed.

Metallographic samples were prepared using cold mounting method to avoid heat treating the materials. Samples were polished and no etching was performed. XY plane of the sample was examined using Scanning Electron Microscope (SEM).

Results and Discussion

Tensile Test

The tensile test result is summarized in Table 4 together with the hardness values. The nominal stress–strain curves are shown in Fig. 2. The AB samples have the highest UTS as expected. Although T6 samples increase the UTS from 205 MPa (solutionized condition) to 296 MPa after the aging process, it is still much lower than the AB samples. The yield strength of T6 samples, however, is higher than the AB samples. This phenomenon was also observed by other researchers [6, 7, 9]. The UTS and YS of T6 samples are both higher compared to SR samples. This makes T6 heat treatment a great choice since in most cases stress relief is required, and parts are rarely used in the as-built state. Compared to stress relief heat treatment, T6 heat treatment can more efficiently remove the residual stress and homogenize the microstructure during the solutionization process, and obtain better UTS and YS. On the other hand, the hardness values are closely related to the UTS.

Table 4 Tensile test result of L-PBF AlSi10Mg under different heat treatment conditions

Sample	Modulus (GPa)	0.2% Yield strength (MPa)	UTS (MPa)	Fracture elongation (%)	Micro hardness (HV)
AB	69.5	220	398	5.1	108
SR	69.5	136	251	18.0	89
SHT	66.5	95	205	15.5	81
T6	70.0	240	296	10.4	93

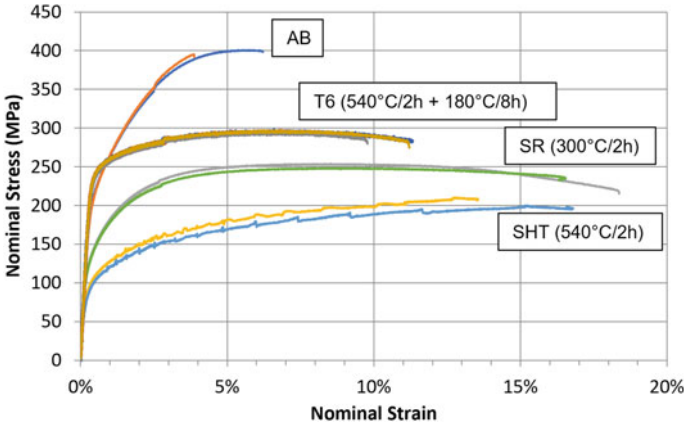


Fig. 2 Tensile nominal stress–strain curves of L-PBF AlSi10Mg under different heat treatment conditions

HCF Results

The fatigue S–N curves are shown in Fig. 3. The solid symbols indicate failures and the hollow symbols indicate runouts. The fitted curves using RFL method described previously are also shown. Table 5 summarizes the fatigue strengths of different samples. Note that the fatigue data for AB samples are from previous study. The sample preparation and testing procedures are similar and can be found in [17].

The number of literatures studying the effect of T6 heat treatment on fatigue strength of L-PBF AlSi10Mg is limited. Due to different laser process parameters, fatigue test method, sample preparation, etc., it is difficult to compare fatigue results from different sources. Table 6 summarizes the room temperature fatigue data of

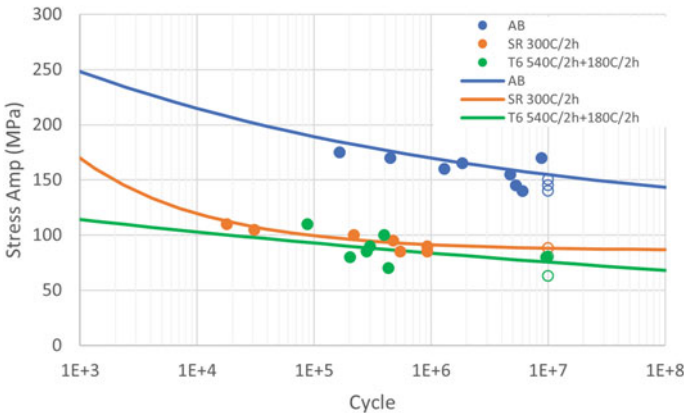


Fig. 3 Fatigue S–N curves of L-PBF AlSi10Mg under different heat treatment conditions

Table 5 Fatigue strengths of L-PBF AlSi10Mg under different heat treatment conditions

Sample ID	Fatigue strength at 10^7 cycles (MPa)
AB	154 ± 9 [17]
SR	88 ± 4
T6	78 ± 9

L-PBF AlSi10Mg available before 2019. The fatigue strengths were re-calculated at 10^7 cycles using the method described in Sect. 3.2 to facilitate direct comparing different data. For comparison purposes, the fatigue strengths were converted to $R = -1$ using Goodman relation [20] if UTS of the material is available. The equation is shown below.

$$S_{f,e} = S_{f,-1} \left(1 - \frac{S_m}{S_{uts}} \right) \quad (2)$$

where $S_{f,e}$ is the equivalent fatigue strength for mean stress S_m . $S_{f,-1}$ is the fatigue strength at $R = -1$ and S_{uts} is the UTS of the material.

Brandl et al. [10] performed a series of fatigue tests at $R = 0.1$ with different sample orientations with/without T6 heat treatment. They found T6 heat treatment significantly improved the fatigue strength for all three orientations (0° , 45° , 90°) with a build plate temperature of 300°C . Maskery et al. [4] also found the similar T6 heat treatment recipe doubled the fatigue strength of the vertically built sample with as-built surface. Ngnekou et al. [12] also found T6 heat treatment improved the fatigue strength of stress relieved vertical and horizontal samples. The data points from Zhang et al. [13] are too few to draw a conclusion on the effect of heat treatment. Bagherifard et al. [14] performed rotating bending fatigue test on samples with as-built surface and concluded that T6 heat treatment significantly improved the fatigue strength. Note that Bagherifard et al. [14] used a much higher solution heat treatment temperature (560°C).

The results from the literatures are contrary to the finding in this study. However, a few subtle testing differences need to be pointed out. Both Maskery et al. [4] and Bagherifard et al. [14] used samples built to net shape without stress relieving. The samples could have significant residual stress which decreases the fatigue strength. This has been observed by Lai et al. [21]. Only Brandl et al. [10] and Ngnekou et al. [12] used samples machined from cylindrical rods, which could result in residual stress removal. Among all the data listed in Table 6, only the data from Ngnekou et al. [12] is the most conclusive since the samples were first stress relieved.

Location Dependency of Hardness

Figure 4a shows the hardness profile of the fatigue sample along the axial direction. The hardness shows a significant location dependency along the build height

Table 6 Fatigue strengths of L-PBF AlSi10Mg reported in literature

Ref	Machine	Plate temp. (°C)	Orient (°)	Sample type	Stress relief	Post heat treatment	Surface cond.	R Ratio	Fatigue strength (R = 1)	Fatigue strength (R = 0.1)	T6 Improves fatigue strength
Brandl et al. [10]	Trumpf TrumaForm LF130	30	0	Round-hourglass		525 °C/6 h + 165 °C/7 h	Machined	0.1	–	90.9 ± 6.0	
		30	90	Round-hourglass		525 °C/6 h + 165 °C/7 h	Machined	0.1	–	40.6 ± 3.2	
		30	45	Round-hourglass		525 °C/6 h + 165 °C/7 h	Machined	0.1	–	37.4 ± 3.0	
		300	0	Round-hourglass			Machined	0.1	–	45.1 ± 4.6	
		300	0	Round-hourglass		525 °C/6 h + 165 °C/7 h	Machined	0.1	–	66.1 ± 1.84	Yes
		300	90	Round-hourglass			Machined	0.1	–	48.7 ± 3.6	
		300	90	Round-hourglass		525 °C/6 h + 165 °C/7 h	Machined	0.1	–	50.9 ± 3.5	Yes
		300	45	Round-hourglass			Machined	0.1	–	44.4 ± 4.0	
		300	45	Round-hourglass		525 °C/6 h + 165 °C/7 h	Machined	0.1	–	70.4 ± 8.3	Yes

(continued)

Table 6 (continued)

Ref	Machine	Plate temp. (°C)	Orient (°)	Sample type	Stress relief	Post heat treatment	Surface cond.	R Ratio	Fatigue strength (R = 1)	Fatigue strength (R = 0.1)	T6 Improves fatigue strength
Maskery et al. [4]	Renishaw AM250	180	90	Round-hourglass			As-built	0.1	29.3	26.4 ± 2.2	
		180	90	Round-hourglass		520 °C/1 h + 160 °C/7 h	As-built	0.1	60.9	54.2 ± 2.2	Yes
Ngnkou et al. [12]	-	150	0	Round-straight	210 °C/1 h		Machined	1	*6		
		200	0	Round-straight	300 °C/2 h		Machined	1	84		
		200	0	Round-straight	300 °C/2 h	540 °C/8 h + 20 °C/24 h + 160 °C/10 h	Machined	1	93		Yes
		200	90	Round-straight	300 °C/2 h		Machined	1	95		
		200	90	Round-straight	300 °C/2 h	540 °C/8 h + 20 °C/24 h + 160 °C/10 h	Machined	1	70		Yes
Zhang et al. [13]	SLM system (LSNF-2)	-	-	Round-straight			Machined	1	95		

(continued)

Table 6 (continued)

Ref	Machine	Plate temp. (°C)	Orient (°)	Sample type	Stress relief	Post heat treatment	Surface cond.	R Ratio	Fatigue strength (R = 1)	Fatigue strength (R = 0.1)	T6 Improves fatigue strength
				Round-straight	300 °C/2 h furnace cool		Machined	1	*74		
				Round-straight		530 °C/1 h	Machined	1	*50		
				Round-straight		530 °C/1 h + 170 °C/12 h	Machined	1	*103		Inconclusive
Bagherifard et al. [14]	SLM500HL	150	90	Round-hourglass			As-built	Rotating bending	50 ± 4		
		150	90	Round-hourglass		560 °C/1 h + 160 °C/6 h	As-built	Rotating bending	75 ± 7		Yes

*The data points are too few to calculate the fatigue strength at 10^7 cycles. The value calculated here is not meaningful

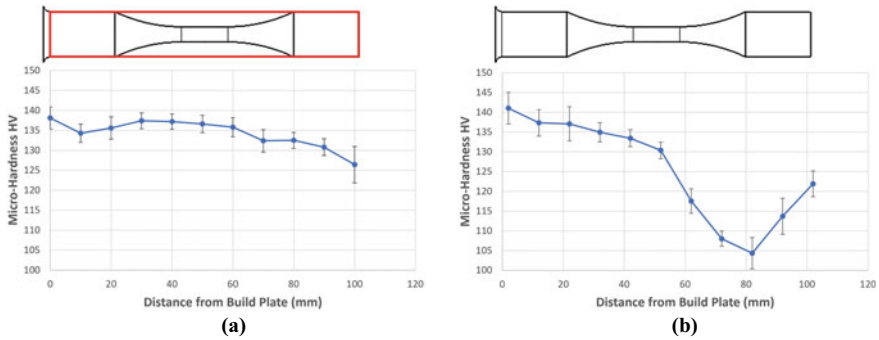


Fig. 4 Hardness profiles of vertically built L-PBF AlSi10Mg. **a** A fatigue sample machined from a straight rod and **b** a fatigue sample built directly into the round dog-bone shape

as it decreases from the bottom to the top. Note that the sample was built into a straight rod, as indicated by the red profile in figure. During the building process, the bottom portion was built first and left in the chamber for hours until the part was completed. This means that the bottom portion of the sample has undergone a heat treatment similar to the aging process. Hitzler et al. [22] also observed the build height dependency of hardness and found the hardness is higher at the bottom than the top of the sample when the build plate temperature was kept at 200 °C during the building process. Hitzler et al. [22] performed a series of experiment and concluded that the hardness difference was due to the thermal exposure during the building process which serves as a T5-like aging. Different build plate temperatures can result in different hardness profile along the axial direction of the sample. For example, Hitzler et al. [22] found that the sample has an overall higher hardness with minimal difference between the top and bottom portions of the sample if the build plate was not heated. However, Buchbinder et al. [23] reported that build plate preheating (220 °C) resulted in lower hardness at the bottom area of the sample.

For simple geometry such as the vertically built straight rod, the hardness follows a decreasing trend from the bottom to the top, as shown in Fig. 4a. However, the hardness shows a complex profile when the sample geometry is irregular. For example, Fig. 4b shows the hardness profile along the axial direction of the fatigue sample that was built directly into the round dog-bone shape (for details of the sample production, refer to [17]). The hardness still follows a decreasing trend from the bottom to the top as observed in Fig. 4a. However, it shows a minimum hardness at around 80 mm from the bottom and the hardness increases after. The results imply that the geometry can also influence the location dependency of hardness by changing the local thermal history. Hitzler et al. [22] observed non-uniform hardness between the border and the center portions of the sample at the same height and attributed to the change in heat dissipation at different locations. The powder surrounding the solid part acts as a heat barrier and forces most of the heat to flow downward through the sample to the build plate. The geometry change in the sample can significantly change the heat

flow pattern and result in different thermal history at different locations. This might be the reason for the distinct hardness profile shown in Fig. 4b.

In summary, the thermal history and the aging process occurring during the building process are very complex and dependent on many variables, ex. heat dissipation rate, build plate temperature, sample height, sample size, sample geometry, build time, etc. It is difficult to know the exact aging response during the building process and predict the final mechanical properties. Thus, the location dependency of mechanical properties needs to be considered and spot checks at critical locations of the parts should be performed to guarantee produce performance.

Artificial Aging

T6 Aging Curves

The T6 heat treatment is composed of solution heat treatment followed by artificial aging. The solution heat treatment temperature ranges between 500 °C to 560 °C. Incipient melting can occur if the temperature is above 560 °C. Solution heat treatment time is typically between 2 to 8 h. In this study, 540 °C for 2 h was selected. The T6 aging curves at 160 °C and 200 °C after solution heat treatment are shown in Fig. 5a. The figure shows that lower aging temperature results in higher peak aged hardness as expected. The peak aging time is around 8 h for both temperatures. After 8 h, the hardness goes down slightly. Both peak aged hardness values of 160 °C and 200 °C aging curves are lower than the hardness in the as-built state.

The aging behavior of L-PBF AlSi10Mg is quite different compared to its sand cast counterpart. Figure 5b shows the T6 aging curve of sand cast AlSi10Mg at 165 °C [24]. Note that the solution heat treatment recipe is 545 °C for 6 h, which is slightly different from the one used in this study. The L-PBF AlSi10Mg shows a delayed aging response compared to sand cast AlSi10Mg, whose hardness peaks at about 1 h. Besides, the peak aged hardness is higher than the one in the as-cast state. The results

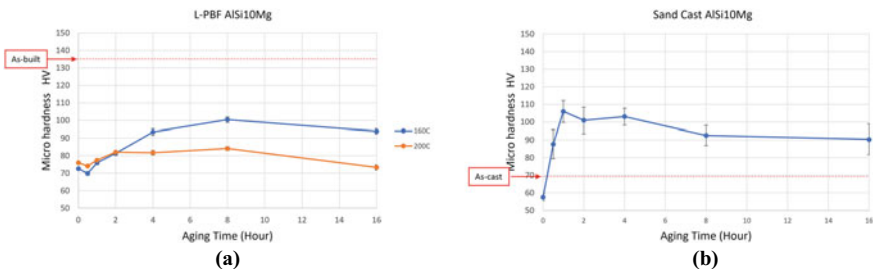


Fig. 5 **a** T6 aging curves at 160 °C and 200 °C for L-PBF AlSi10Mg. Samples were solutionized at 540 °C for 2 h before aging. **b** T6 aging curves at 165 °C for sand cast AlSi10Mg. Samples were solutionized at 545 °C for 6 h before aging. [24]

show that the T6 heat treatment recipe needs be tailored to AlSi10Mg produced by L-PBF process. Recipes used for the same/similar materials produced by conventional methods might not be suitable for L-PBF AlSi10Mg. This can be attributed to the complex nature of thermal history and aging response during the building process. For example, Casati et al. [25] found that the build plate temperature can dramatically change the aging response for L-PBF AlSi10Mg. The sample showed a significant hardness increase after aging at 160 °C (T5 heat treatment) when the build plate was not heated during the building process. On the other hand, the sample showed a hardness decrease after aging at 160 °C (T5 heat treatment) when the build plate was kept at 160 °C during the building process. One should make sure the T6 recipe produces desired aging response and mechanical properties.

T5 Aging Curves

The T5 heat treatment is composed of artificial aging only. Due to the hardness difference observed in the sample (discussed in Sect. 3.3), sections from different locations of the dog-bone samples were aged at the same time see if difference in aging response exists. Figure 6 shows the name and location of each section used in the T5 aging study. The red contour shows the straight rod geometry before machining into the dog-bone geometry. As shown in Fig. 7, aging at 120 °C does not seem to have an effect on L-PBF AlSi10Mg up to 400 h since the temperature is relatively low. Although the top section seems to have a slight hardness increase after 100 h, the increase is small and the aging time is too long. Figure 8a, b shows the aging curves at 150 °C for top and near top sections for 2 samples, respectively. The top sections seem to exhibit an aging response and peak around 20 h. The near top sections, however, do not show a noticeable increase and the hardness decreases after 20 h. Figure 9 shows the aging curves at 200 °C at various locations of a sample. The near top section shows the lowest hardness before aging, which coincides with the finding in Fig. 4b for samples built directly into dog-bone shape. Note that the top section shows a slight hardness increase, which was also observed in samples aged at 120 °C and 150 °C. On the other hand, the bottom section shows a hardness decrease. The different aging response at different locations of a sample was observed

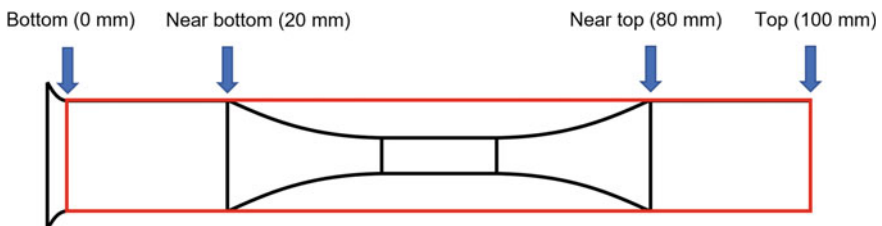


Fig. 6 Names and locations of the sections in the dog-bone sample used in T5 aging study. The red profile shows the as-built straight rod

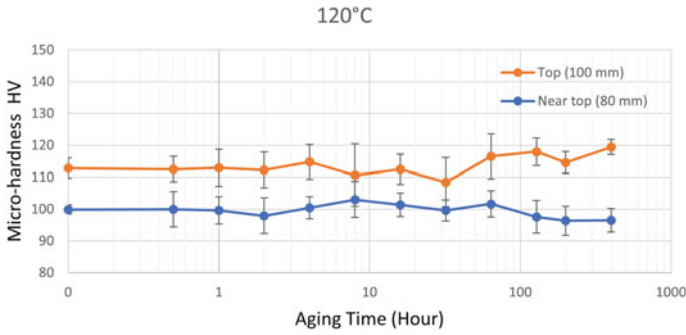


Fig. 7 T5 aging curves at 150 °C for L-PBF AlSi10Mg. a Top and b near top sections

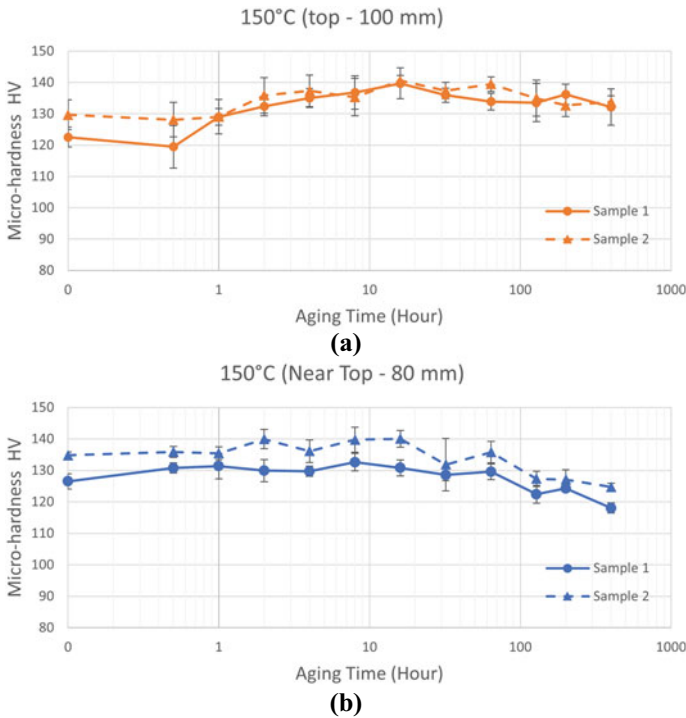


Fig. 8 T5 aging curves at 150 °C for L-PBF AlSi10Mg. a Top and b near top sections

by Hitzler et al. [22], which was mentioned earlier in Sect. 3.3. The top section does not experience the thermal exposure during the building process and thus shows a typical T5 aging response. The bottom section has gone through long hours of thermal exposure which has peak aged or over aged the material. Hence the hardness decreases as it enters the overaging phase.

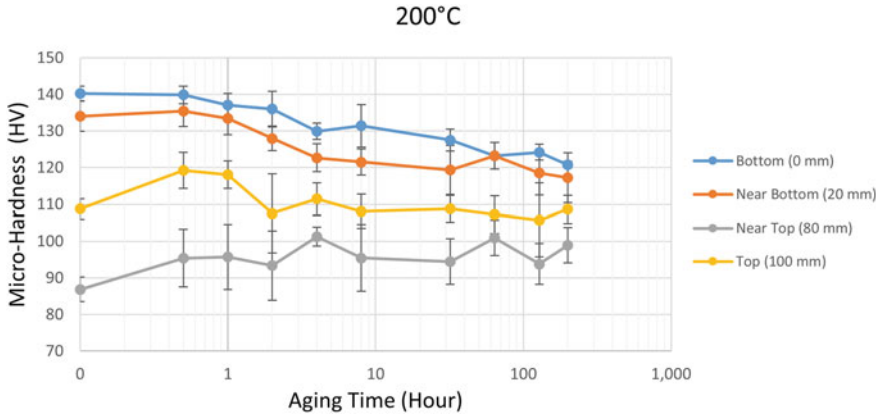


Fig. 9 T5 aging curves at 200 °C for L-PBF AlSi10Mg

Overall, the T5 aging does not provide significant strength improvement. Temperature within this range (120 °C and 200 °C) cannot remove the residual stress in the as-built part either. Thus, it is concluded that T5 aging is not suitable for L-PBF AlSi10Mg.

Thermal Exposure

Based on the results in Sect. 3.4.2, it is concluded that the mechanical properties are relatively stable when the temperature is below 200 °C. In certain powertrain applications, the environmental temperature can be higher than 200 °C. Understanding the thermal stability is then critical. Figure 10 shows that hardness change versus time at 250 °C and 300 °C for L-PBF AlSi10Mg. Note that the samples used in the study

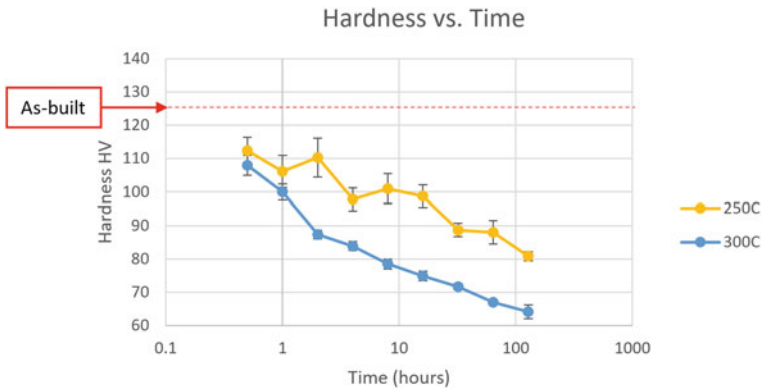


Fig. 10 Hardness change versus time at 250 °C and 300 °C for L-PBF AlSi10Mg

are made in SLM125 from previous study and have a higher hardness in the as-built state [17]. It is clear that the hardness decreases dramatically at these temperatures and does not seem to stabilize at 128 h. Further hardness decrease is highly likely if the thermal exposure continues at these temperatures. The hardness decrease can be attributed to the significant silicon eutectic coarsening observed in the literatures [3]. The significant softening needs to be considered if the parts are to be used at elevated temperatures.

Silicon Eutectic Morphology Evolution during T5 Aging

The objective of this study is to understand the thermal stability of the silicon eutectic structure at elevated temperatures and its relation to the hardness change during the T5 aging process. Figures 11, 12 and 13 show the microstructure of sections of samples aged under T5 condition at different temperatures. Note that the microstructure shown in the figures are all from the weld pool center to facilitate direct comparison. Figure 11 shows the top and near top sections before and after 400 h of aging at 120 °C. The corresponding aging curves are shown in Fig. 7. The silicon eutectic does not show a noticeable difference between the top and near top sections before aging. After aging for 400 h, the smooth silicon eutectic cell walls became slightly irregular, and some silicon precipitated from the aluminum matrix. However, the silicon eutectic cell size and structure do not change much. Figure 12 shows the top and near top sections before and after aging at 150 °C. The corresponding aging curves are shown in Fig. 8 sample 2. The silicon eutectic does not show a noticeable difference between the top and near top sections before aging, nor between the 0-h, 32-h, and 400-h aged samples. Figure 13 shows the near top sections before and after aging at 200 °C, and the bottom section before aging. The corresponding aging curves are shown in Fig. 9. The silicon eutectic does not show a noticeable difference between the near top and bottom sections before aging, nor between the 0-h and 200-h aged near top sections. The top and bottom sections also show similar eutectic cell size, which means the hardness difference seen in Fig. 9 is not related to the silicon eutectic morphology.

In summary, T5 aging between 120 °C and 200 °C does not change the silicon eutectic morphology. The small hardness change, either increase or decrease, during the T5 aging process is mainly from precipitation in this temperature range, as discussed in the literature [22, 25].

Conclusions

The effect of common post heat treatments, i.e. stress relief, solution heat treatment, T5 and T6 aging, on mechanical properties of L-PBF AlSi10Mg was investigated. Below summarizes the important findings and conclusions.

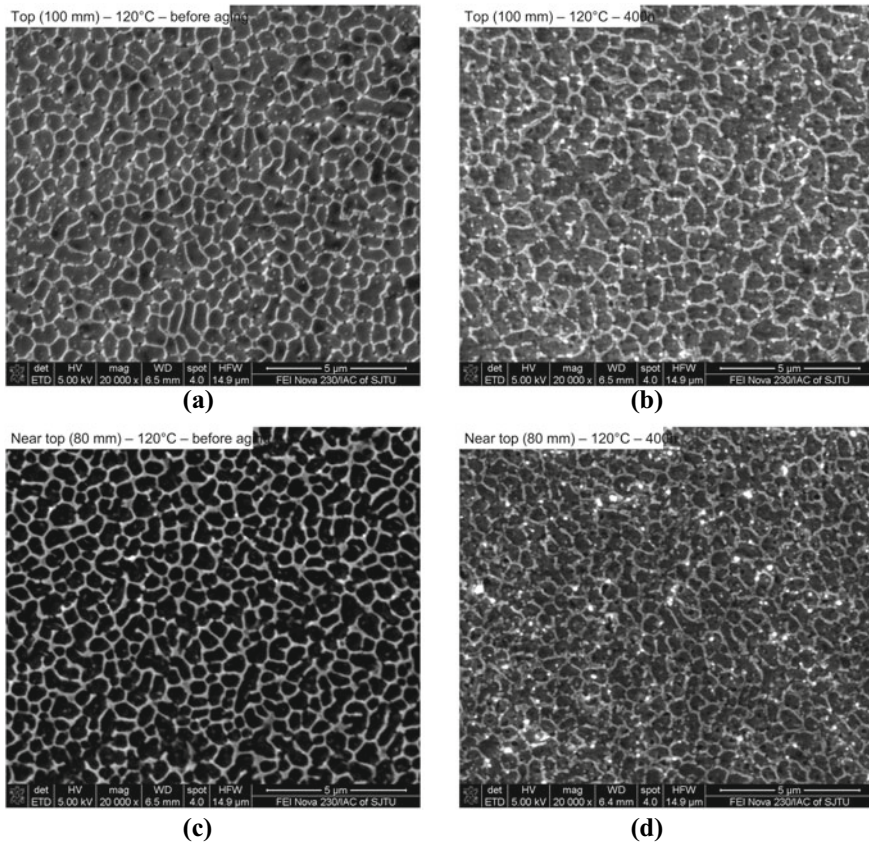


Fig. 11 Silicon eutectic morphology at the weld pool center of top section (a) before T5 aging and (b) T5 aged for 400 h at 120 °C; near top section (c) before T5 aging and (d) T5 aged for 400 h at 120 °C

1. As-built samples have the highest UTS. T6 samples have the highest YS and better elongation compared to as-built samples. Stress relieved samples have much lower YS and UTS compared to as-built and T6 samples.
2. Since stress relief is required in most cases, T6 heat treatment is a good solution to restore some of the YS and UTS to have balanced mechanical properties.
3. As-built samples have the highest fatigue strength provided that no residual stress was present. Both stress relieved and T6 samples show much lower fatigue strength compared to as-built samples.
4. The fatigue strength of T6 and stress relieved samples do not follow UTS nor hardness trends that was commonly used for fatigue strength estimation.
5. Hardness is location dependent in the as-built part. The hardness is higher at the bottom of the sample in this study. However, no significant difference in silicon eutectic cell size was observed between the bottom and top of the sample. The

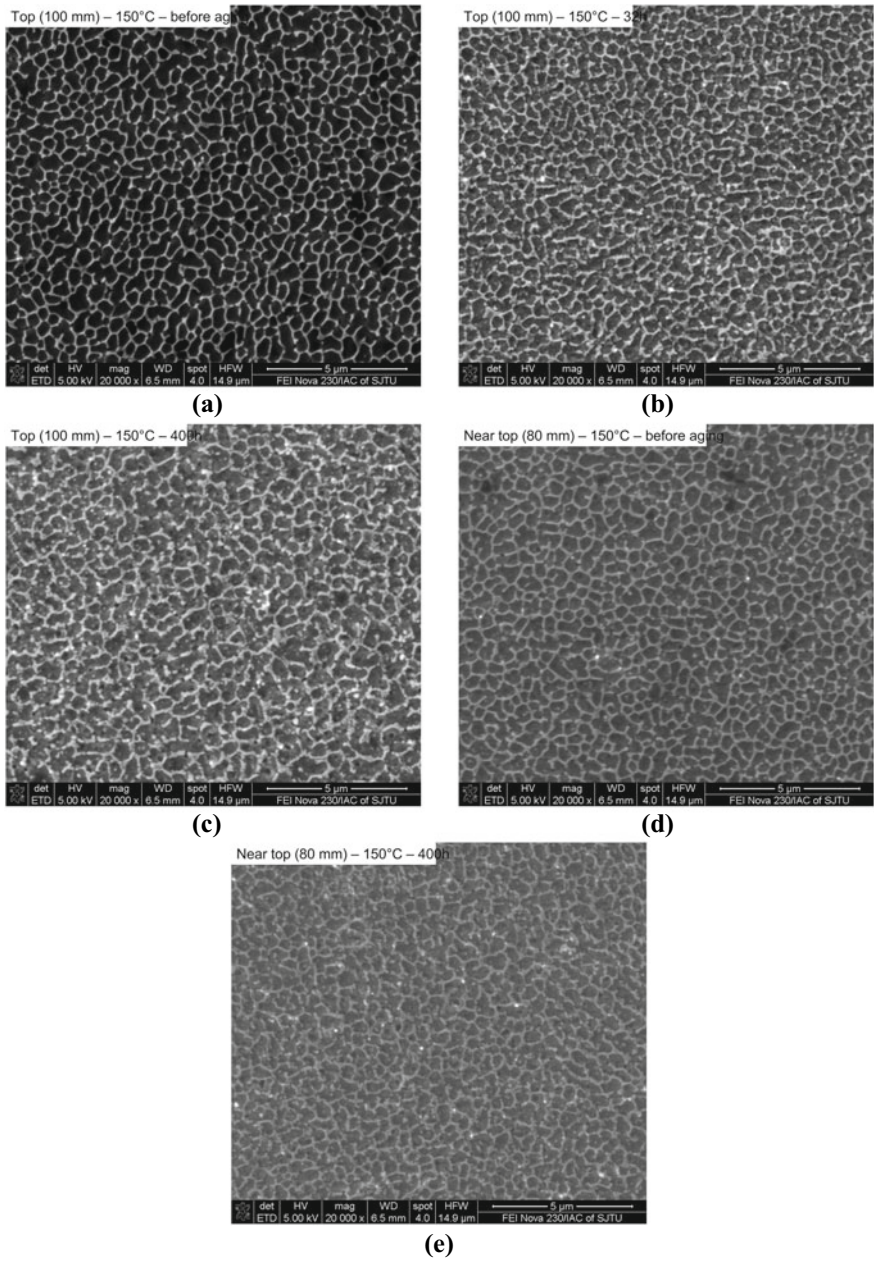


Fig. 12 Silicon eutectic morphology at the weld pool center of top section (a) before T5 aging, (b) T5 aged for 32 h, and (c) T5 aged for 400 h at 150 °C; near top section (d) before T5 aging and (e) T5 aged for 400 h at 150 °C

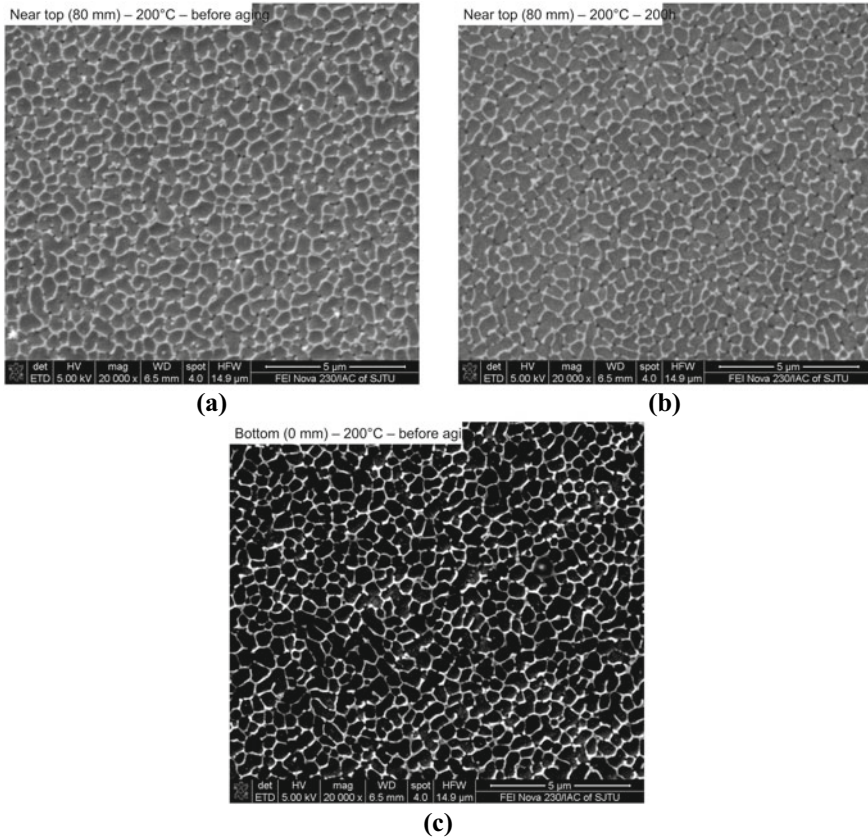


Fig. 13 Silicon eutectic morphology at the weld pool center of near top section (a) before T5 aging and (b) T5 aged for 200 h at 200 °C; (c) bottom section before T5 aging

cause of the hardness difference is linked to the thermal exposure which acts as T5-like aging during the building process. The part geometry can also change the thermal pattern within the sample which further complicates the hardness difference.

6. Minor aging behavior was observed under T5 aging at 120 °C, 150 °C, and 200 °C up to 400 h. Silicon eutectic morphology does not show significant change after T5 aging at these temperatures.
7. T6 aging at 160 °C and 200 °C shows moderate hardness increase compared to solutionized samples, but still much lower than the as-built samples.

References

1. Aboulkhair NT, Tuck C, Ashcroft I, Maskery I, Everitt NM (2015) On the precipitation hardening of selective laser melted AlSi10Mg. *Metall Mater Trans A* 46:3337–3341. <https://doi.org/10.1007/s11661-015-2980-7>
2. Li W, Li S, Liu J, Zhang A, Zhou Y, Wei Q, Yan C, Shi Y (2016) Effect of heat treatment on AlSi10Mg alloy fabricated by selective laser melting: microstructure evolution, mechanical properties and fracture mechanism. *Mater Sci Eng, A* 663:116–125. <https://doi.org/10.1016/j.msea.2016.03.088>
3. Takata N, Kodaira H, Sekizawa K, Suzuki A, Kobashi M (2017) Change in microstructure of selectively laser melted AlSi10Mg alloy with heat treatments. *Mater Sci Eng, A* 704:218–228. <https://doi.org/10.1016/j.msea.2017.08.029>
4. Maskery I, Aboulkhair NT, Tuck C, Wildman RD, Ashcroft IA, Everitt NM, Hague RJM (2015) Fatigue performance enhancement of selectively laser melted aluminium alloy by heat treatment. In: Paper presented at the 26th annual international solid freeform fabrication symposium—an additive manufacturing conference, Austin, Texas, 10–12 August 2015
5. Kimura T, Nakamoto T (2014) Microstructures and mechanical properties of Al–10%Si–0.4%Mg fabricated by selective laser melting. *J Japan Soc Powder Powder Metall* 61(11):531–537. <https://doi.org/10.2497/jjpspm.61.531>
6. Zhou L, Mehta A, Schulz E, McWilliams B, Cho K, Sohn Y (2018) Microstructure, precipitates and hardness of selectively laser melted AlSi10Mg alloy before and after heat treatment. *Mater Charact* 143:5–17. <https://doi.org/10.1016/j.matchar.2018.04.022>
7. Fousová M, Dvorský D, Michalčová A, Vojtěch D (2018) Changes in the microstructure and mechanical properties of additively manufactured AlSi10Mg alloy after exposure to elevated temperatures. *Mater Charact* 137:119–126. <https://doi.org/10.1016/j.matchar.2018.01.028>
8. Kempen K, Thijs L, Humbeeck JV, Kruth J-P (2015) Processing AlSi10Mg by selective laser melting: parameter optimisation and material characterisation. *Mater Sci Tech* 31(8):917–923. <https://doi.org/10.1179/1743284714Y.0000000702>
9. Tradowsky U, White J, Ward RM, Read N, Reimers W, Attallah MM (2016) Selective laser melting of AlSi10Mg: influence of post-processing on the microstructural and tensile properties development. *Mater Des* 105:212–222. <https://doi.org/10.1016/j.matdes.2016.05.066>
10. Brandl E, Heckenberger U, Holzinger V, Buchbinder D (2012) Additive manufactured AlSi10Mg samples using Selective Laser Melting (SLM): microstructure, high cycle fatigue, and fracture behavior. *Mater Des* 34:159–169. <https://doi.org/10.1016/j.matdes.2011.07.067>
11. Murakami Y (2002) *Metal fatigue: effects of small defects and nonmetallic inclusions*. Elsevier, London, UK
12. Ngnenkou JND, Nadot Y, Henaff G, Nicolai J, Kan WH, Cairney JM, Ridosz L (2019) Fatigue properties of AlSi10Mg produced by additive layer manufacturing. *Int J Fatigue* 119:160–172. <https://doi.org/10.1016/j.ijfatigue.2018.09.029>
13. Zhang C, Zhu H, Liao H, Cheng Y, Hu Z, Zeng X (2018) Effect of heat treatments on fatigue property of selective laser melting AlSi10Mg. *Int J Fatigue* 116:513–522. <https://doi.org/10.1016/j.ijfatigue.2018.07.016>
14. Bagherifard S, Beretta N, Monti S, Riccio M, Bandini M, Guagliano M (2018) On the fatigue strength enhancement of additive manufactured AlSi10Mg parts by mechanical and thermal post-processing. *Mater Des* 145:28–41. <https://doi.org/10.1016/j.matdes.2018.02.055>
15. ASTM International (2011) ASTM E8–11 Standard test methods for tension testing of metallic materials. ASTM International, West Conshohocken
16. ASTM International (2007) ASTM E466–07 Standard practice for conducting force controlled constant amplitude axial fatigue tests for metallic materials. ASTM International, West Conshohocken
17. Lai W, Li Z, Ojha A, Li Y, Forsmark J, Engler JC, Su X (2020) Effects of surface roughness and porosity on fatigue behavior of AlSi10Mg produced by laser powder fusion process. In: Paper presented at 4th ASTM symposium on structural integrity of additive manufactured

- materials and parts, Oxon Hills, MD, USA, 7–10 October 2019. <https://doi.org/10.1520/STP163120190127>
18. Pascual FG, Meeker WQ (1999) Estimating fatigue curves with the random fatigue-limit model. *Technometrics* 41:277–290. <https://doi.org/10.2307/1271342>
 19. Engler-Pinto C, Lasecki J, Frisch R, DeJack M, Allison J (2005) Statistical approaches applied to fatigue test data analysis. In: Paper presented at the SAE 2005 world congress & exhibition, Detroit, MI, USA, 11–14 April 2005
 20. Bannantine JA, Comer JJ, Handrock JL (1990) *Fundamentals of metal fatigue analysis*. Prentice Hall, New Jersey
 21. Lai W, Ojha A, Li Z, Engler-Pinto C, Su X (2021) Effect of residual stress on fatigue strength of 316L stainless steel produced by laser powder bed fusion process. *Progr Addit Manuf* 6:375–383. <https://doi.org/10.1007/s40964-021-00164-8>
 22. Hitzler L, Janousch C, Schanz J, Merkel M, Heine B, Mack F, Hall W, Öchsner A (2017) Direction and location dependency of selective laser melted AlSi10Mg specimens. *J Mater Process Technol* 243:48–61. <https://doi.org/10.1016/j.jmatprotec.2016.11.029>
 23. Buchbinder D, Meiners W, Wissenbach K, Poprawe R (2015) Selective laser melting of aluminum die-cast alloy—correlations between process parameters, solidification conditions, and resulting mechanical properties. *J Laser Appl* 27(S2):9205. <https://doi.org/10.2351/1.4906389>
 24. Lai W, Ojha A, Li Z (2020) Effect of as-cast surface roughness on fatigue strength of sand cast AlSi10Mg aluminum alloy. Ford Motor Company internal technical report
 25. Casati R, Hamidi Nasab M, Coduri M, Tirelli V, Vedani M (2018) Effects of platform pre-heating and thermal-treatment strategies on properties of AlSi10Mg alloy processed by selective laser melting. *Metals* 8(11):954. <https://doi.org/10.3390/met8110954>